Soft Matter

Accepted Manuscript

ROYAL SOCIETY OF CHEMISTRY

rsc.li/soft-matter-journal

View Article Online
DOI: 10.1039/D6SM00119J

Formation of assembloids by DNA-mediated synthetic cell self-assembly

Anna Burgstaller[1,2,3*] Erick Angel Lopez Lopez[1], Gyu-Min Hwang[1], Kevin Jahnke[4,5], Oskar Staufer[1,2,3,6*]

1 INM – Leibniz Institute for New Materials Campus D2 2, 66123 Saarbrücken, Germany
2 Helmholtz Institute for Pharmaceutical Research Saarland Helmholtz Center for Infection Research Campus E8 1, 66123 Saarbrücken, Germany
3 Saarland University, Center for Biophysics, Campus Saarland, 66123 Saarbrücken, Germany
4 School of Engineering and Applied Sciences, Harvard University, 02138 Cambridge, MA, USA
5 Biomembrane Engineering Group, Max Planck Institute for Medical Research at Bildungscampus Heilbronn, 74076 Heilbronn, Germany
6 Max Planck Bristol Centre for Minimal Biology, Cantock's Close, Bristol BS8 1TS, UK

*Corresponding author: oskar.staufer@leibniz-inm.de; anna.burgstaller@leibniz-inm.de

Keywords: Bottom-up synthetic biology, synthetic cells, tissue engineering, immuno-biophysics, DNA nanotechnology

Abstract: Approaches in tissue engineering, organoid culture, and organs-on-chip have propelled the development of increasingly sophisticated *in vitro* models of human tissues. However, as they are formed from natural cells, it is challenging to control their molecular composition and biophysical properties, increasing variability, and limiting their robustness. To overcome these limitations, we introduce a self-assembly strategy for synthetic cells that enables the formation of millimeter-sized synthetic constructs based on single synthetic cells. Specifically, we functionalize the lipid membrane of synthetic cells with cholesterol-tagged single-stranded DNA aptamers, which drive programmable intercellular adhesion through sequence-specific hybridization. This allows individual synthetic cells to interconnect into higher order 3D constructs. By varying aptamer complementarity, internal architecture with spatially distinct functional zones and tuneable mechanical properties can be encoded. Most importantly, the DNA-driven self-assembly operates directly in cell culture medium, is compatible with high-throughput microwell formats enabling scalable screening workflows and

View Article Online
DOI: 10.1039/D6SM00119J

is reversible by DNA displacement. To demonstrate biological functionality of these synthetic tissues, we incorporate T cell-stimulatory antibodies into spatially segregated tissue regions. This design mimics lymph node organization and supports infiltration of natural primary human T cells, which subsequently expand within the synthetic tissue. Together, these results establish a route to tissue-scale matrices built from synthetic cell collectives and represent a critical step toward functionally integrating living and non-living matter.

Introduction

Synthetic tissue constructs are defined as minimalistic replicas of natural tissues, mimicking their functional and structural properties, which are built not from natural but from individual synthetic cells [1]. Similar to natural tissues, their functional properties arise from their biochemical, mechanical and structural characteristics, which are emergent properties from the synthetic cell collective [2]. The research field of synthetic cell engineering received significant attention in the last decades and achieved several critical milestones. For example, giant unilamellar vesicles (GUVs) were designed to act as functional immune-inspired synthetic cells with adoptable lipid membrane [3] or to serve as cargo transport system [4]. Colloidosomes, synthetic cells with a semipermeable silica membrane surrounding an aqueous core, have been designed to receive and react to chemical signals as well as to reconstitute minimalistic metabolic processes [5]. Other examples for synthetic cell systems include coacervates, formed by liquid-liquid phase separation, which can act as membraneless synthetic organelles within a membrane-based synthetic cells [6, 7]. In our previous work we developed synthetic cells termed droplet supported lipid bilayer (dsLBs) composed of a lipid bilayer membrane which is supported by a polydimethylsiloxane (PDMS) oil core. DsLBs cover a tuneable stiffness range from ~1 kPa to ~3000 kPa by varying by varying their internal oil core cross-linking degree. The dsLB lipid membrane is a lateral mobile bilayer, as confirmed by nitrobenzoxadiazole assay, cryoTEM and fluorescent recovery after photobleaching. DsLB have sizes of 3.75 µm (±2.61 µm) and PDI of 0.58. To achieve biochemical functionality, the

View Article Online
DOI: 10.1039/D6SM00119J

dsLB membrane can be functionalized with antibodies and other proteins for controlled interactions with living cells, including activation and proliferation of high-quality T cells and hybrid spheroids [8, 9].

Synthetic cells are generally considered to have high translational potential for application in biomanufacturing, advanced cell culturing and tissue engineering [10]. However, following this realm, transforming synthetic cell technologies from dispersed synthetic cell solution to condensed organized synthetic cell collectives in 3D formats, remains a major frontier in the field [1]. Importantly, adding such a 3D characteristic to advanced cell culture systems has previously proven to be a major advantage for natural cell cultures, most prominently in stem cell and oncogenesis analysis [11-14], where organoids have become powerful and highly relevant model systems. The field is now progressing even further, from generating individual organoids that replicate specific tissue structures to creating assembloids, which integrate multiple organoid types into coherent, multifunctional constructs that better capture the complexity of living organs[15].

Formation of multicellular 3D synthetic assembloids from synthetic cells remains challenging as this requires three main features that need to be integrated: biochemical functionality, hierarchical organization and physiological biomechanical properties [16]. Looking at natural cell cultures, matrigel has been a gold standard to mimic exclusively the extracellular matrix (ECM) properties of tissues for studies concerning embryonic or malignant cells [17, 18]. Even though this system is tuneable to some degree in terms of integrated growth factors, proteins, enzymes or structural components such as collagen [19], it is limited by batch-to-batch variability [20]. Many naturally derived 3D culture systems share these limitations [21].Therefore, synthetic cells could meet this need to form synthetic constructs from the bottom-up to introduce more controllability, reliability and tunability to 3D culture systems thereby not only mimicking the ECM component of tissues but also cells in a tissue environment.

View Article Online
DOI: 10.1039/D6SM00119J

3D culturing systems are particularly attractive for *ex vivo* expansion of T cells, which is a critical step in adoptive cell therapy. Therefore, several 3D systems have been developed to culture, activate and expand T cells. These include synthetic hydrogels that can be tuned in their crosslinking degree leading to different stiffnesses [22] or equipped with biochemical cues such as immune cell stimulating beads [23]. Even though hydrogels offer many advantages such as their degradability, viscoelasticity and bioprinting compatibility [24-27], hydrogels are bulk polymer networks that omit mimicry of cells within a tissue complex and the hierarchical microanatomy of tissues. We therefore recently engineered dsLB-based syntactic cells to form 3D synthetic tissues which are able to interact with natural T cells [28]. The self-assembly is based on cross-linking individual synthetic cells *via* biotin-conjugated lipids in their membrane with streptavidin [21]. This allows to introduce hierarchical structure and tissue-like mechanical properties. When integrated with T cell-agonistic antibodies, the resulting millimeter-sized 3D lymphatic bottom-up tissues (lymphBUTs) act as minimalistic, controllable and tuneable natural lymph node replicas into which T cells can infiltrate, migrate, activate and differentiate into regulatory-like $CD8^+$ T cells [21].

However, streptavidin-biotin-based lymphBUTs are still limited in three key features. 1) Their size is limited due to the formation process, thus leading to relatively small constructs with diameters of approximately 2-3 mm, which is smaller than many physiological tissue architectures. 2) Routinely used cell culture media contains soluble biotin, which interferes with streptavidin-based synthetic cell cross-linking, conventional lymphBUTs cannot be formed in cell culture medium. This limits their integration with living cell handling technologies based on bioprinting or organs-on-chip. 3) The formation of lymphBUTs with different reactions zones, in analogy to natural tissues, where different cell types form microphysiological environments (e.g. B cell and T cell zones in the lymph node), is only possible by mixing pre-formed synthetic cell clusters without control over the final spatial arrangements and their sizes. This does not allow to form constructs with more than two different zones, much less than most natural tissues.

View Article Online
DOI: 10.1039/D6SM00119J

We reasoned that using single stranded DNA (ssDNA) instead of multivalent streptavidin as an intercellular adhesion protein analogue to interlink individual synthetic cells could overcome the limitations detailed above [29, 30]. Moreover, new DNA-based formation techniques allow for continuous growth of constructs to larger sizes. Also, self-assembly of dispersed synthetic cells *via* DNA hybridization can be performed in physiological, high ionic strength buffers such as cell culture media. Furthermore, by using ssDNA strands of varying complementary individual zones can be formed under controlled conditions. Lastly, controlled disassembly of 3D constructs was achieved by providing higher affinity displacement stands thus restoring the status of dispersed synthetic cells. Therefore, we established formation of constructs based on ssDNA and evaluated their structure and function as assembloids for *ex vivo* T cell expansion.

Results

Construct formation *via* ssDNA

To leverage the advantage of single-stranded DNA (ssDNA) as selective synthetic cell intercellular adhesion protein analogue, we first integrated ssDNA in the dsLB membrane *via* a cholesterol anchor. The 20bp long anchor strand was subsequently coupled to a partly complementary ssDNA (linker strand - linker 1a, linker 1b) **(Figure 1 A)** to interconnect dsLBs and form constructs **(Figure 1 B, C)**. During ssDNA-based formation of these constructs we achieved significantly larger sizes of individual constructs then for our previous biotin-based ones. The new assembly strategy, which allows construct formation by sedimentation-based contact formation between individual dsLBs, evades mechanical stress by orbital mixing which allows for the formation of bigger-sized constructs. We compared construct sizes between the two formation approaches, confirming that ssDNA-based constructs **(Figure 1 C)**. We first verified the integration of the anchor 20bp-Cy5 strand into the dsLB membrane and subsequent linker 1a 20bp-Cy3 strand hybridization by flow cytometry. Varying ssDNA concentrations were tested in the range of 3 mol% to 15 mol% with the corresponding linker

View Article Online
DOI: 10.1039/D6SM00119J

ssDNA in an equimolar ratio. Quantification of the mean fluorescence intensity (MFI) showed robust integration across all concentrations tested **(Figure 1 D)**. Integrating the anchor ssDNA did also not lead to phase separation in the dsLB lipid bilayer membrane indicated by a homogenous fluorophore distribution in the membrane shown in the confocal microscopy images **(Figure 1 E)**. Most importantly, when ssDNA functionalized dsLBs were incubated in Eppendorf tubes, they spontaneously formed millimeter-sized free-floating constructs (**Figure S 1 A)**. When dsLBs were incubated without linker strands (anchor strands only), no construct formation was observed, demonstrating the specific DNA-paring between the individual synthetic cells as a requirement for the self-assembly (**Figure S 1 C**).

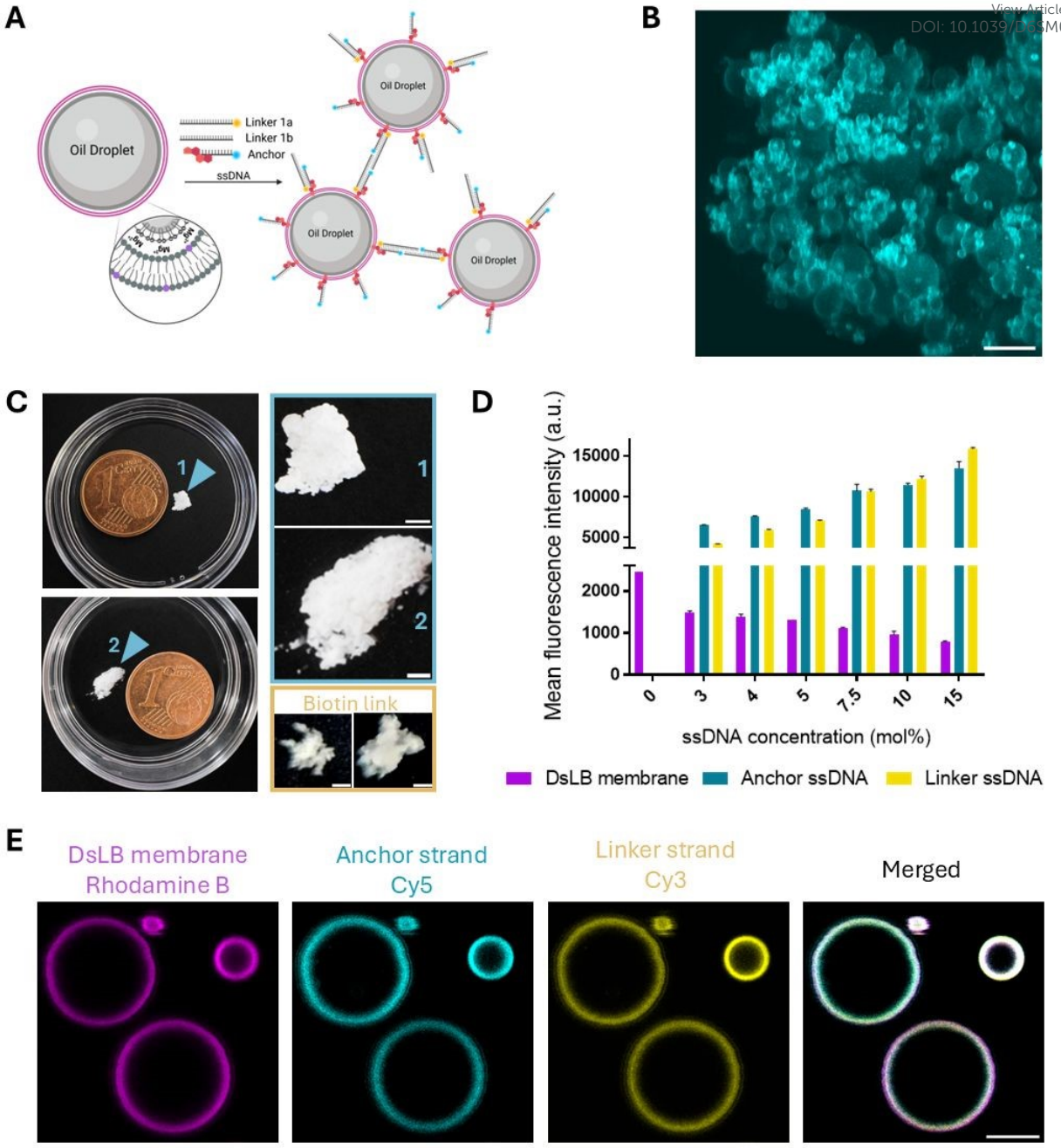

Figure 1: Establishment of a construct formation strategy using ssDNA A) Schematic illustration of inter-dsLB binding *via* partly complementary ssDNA. **B)** Representative confocal microscopy maximal z-projection showing a construct assembled from individual dsLBs using 20bp ssDNA (dsLB membrane: Cy5). Scale bar is 20 µm. **C)** Top view of representative constructs formed *via* ssDNA hybridization (blue) or biotin-streptavidin bond (yellow) [21] next to a 16.25 mm diameter 1 Eurocent for size. Scale bars 1 mm. **D)** Flow cytometry-based quantification of mean fluorescence intensities of the dsLB membrane (Atto 488 lipids), anchor 20bp ssDNA (Cy5) and linker 1a 20bp ssDNA (Cy3) at different concentration of ssDNA including 3 mol%, 4 mol%, 5 mol%, 7.5 mol%, 10 mol% and 15 mol%. Results are shown as mean SD, from 2 replicates. **E)** Representative confocal microscopy image of single dsLBs (Rhodamine B lipid in membrane) decorated with anchor 20bp ssDNA (cyan – Cy5) and linker 1a 20 bp ssDNA (yellow – Cy3). Scale bar is 5 µm.

We next evaluate the integration of ssDNA with varying length by testing 15bp and 25bp strands. We define the ssDNA length by the number of complementary nucleotides between

View Article Online
DOI: 10.1039/D6SM00119J

anchor and linker strands (**Table 1**). The MFIs of the dsLB membrane and the anchor ssDNA were measured by flow cytometry. Individual synthetic cells demonstrate successful ssDNA integration in both cases (**Figure 2 A**). Of note, the shorter ssDNA strands (15bp) showed lower MFI for the ssDNA, while displaying higher MFI for the Rhodamine B fluorophore attached to the head group of 1 mol% of the lipids in the dsLB membrane (**Figure S 1 B**). This is indicative for a static quenching effect between DNA and the membrane fluorophore due to proximity [31, 32]. Integration of ssDNA of both lengths was further confirmed by confocal microscopy images (**Figure 2 B**).

Importantly, construct formation was observed with ssDNA of both lengths (15bp and 25bp) while no formation was detected with only the corresponding anchor stands **(Figure 2 C, Figure S 1 D)**. The main objective of using DNA as a synthetic cell cross-linker is that complementarity and oligo length can be applied to program the self-assembly as well as generating constructs and assembloids with spatially defined biochemical and potential biomechanical properties. We reasoned that the number of inter-dsLB connections (ssDNA concentration) could impact the overall synthetic tissue stiffness as we previously observed for biotin-streptavidin connections [21]. Therefore, we evaluated the mechanical properties of the constructs by microplate parallel compression analysis. For this, constructs formed with either 15bp, 20bp or 25bp and 3 mol%, 5 mol% or 10 mol% ssDNA were produced. The maximal compression force required to compress 10% of the total construct height was measured **(Figure 2 D)**. The measurements indicate that ssDNA concentrations between 3 mol% and 10 mol% have a minor impact on the mechanical properties of the constructs. However, constructs assembled with shorter ssDNA strands (15bp) tend to increase the stiffness with higher ssDNA concentration beginning at 10 mol% in the dsLB membrane. Contrary, the ssDNA concentration does not affect the stiffness of constructs formed with longer ssDNA (20bp and 25bp) **(Figure 2 E - G)**. We additionally tested constructs formed with 20bp ssDNA and ssDNA concentrations of 2 mol% and 20 mol% and detected significantly lower compression force needed to compress 10% of the total construct height, indicating reduced total construct stiffness (**Figure S 1 E**). To optimally balance cost efficacy and construct stability, we chose 5

View Article Online
DOI: 10.1039/D6SM00119J

mol% and 20bp ssDNA length for next experiments. The decreased stiffness for 2 and 20 mol% is potentially rooted in the fact that compressibility is mostly a function of the number of interactions between individual dsLBs in the construct and not necessarily of their binding strength [21]. Of note, the observed variations in compression force in all conditions are, among other factors, a result of the construct orientation.

We further aimed to verify that construct formation *via* ssDNA can be performed in serum-supplemented cell culture medium, in contrast to streptavidin-based lymphBUTs. For this, the ssDNA functionalized synthetic cell suspensions were diluted into RPMI 1640 cell culture medium and construct formation was observed (**Figure S 1 F**). This enables the integration of natural cells into biochemically functionalized constructs further, referred to as synthetic tissues, under physiological environments and opens the door for cell handling procedures such as bioprinting or organs-on-chip.

Next, we aimed to explore the potential to perform DNA-based operations with the constructs to alter structure or function *in situ*. Several operations, including allosteric gates, hybridization chain reactions or strand displacement can be performed with DNA. We implemented strand displacement for switchable disassembly of constructs. For this we added competing linker DNA with higher affinity (dis strand) to the constructs formed with anchor 20bp + linker 11bp 1a/1b or 13bp mm 1a/1b to displace 200% of the original linker DNA. By confocal time lapse microscopy, we observed total disassembly of the constructs within 10 min (**Figure S 1 G**).

View Article Online
DOI: 10.1039/D6SM00119J

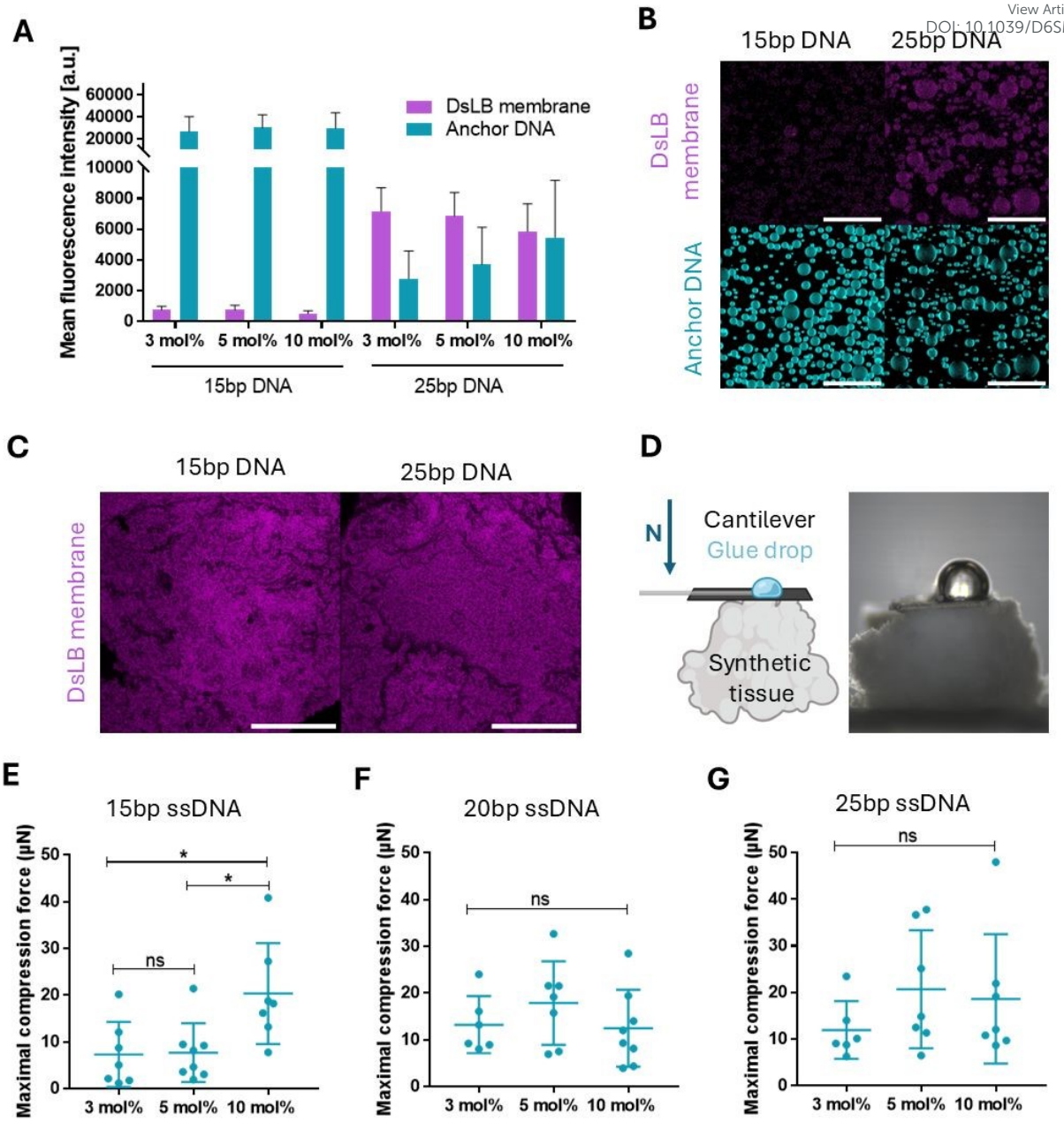

Figure 2: Mechanical properties of ssDNA-based constructs A) Flow cytometry measurements showing the mean fluorescence intensity of dsLBs (magenta) equipped with anchor ssDNA with 15bp and 25bp at different ssDNA concentrations of 3 mol%, 5 mol% and 10 mol%. **B)** Representative confocal microscopy z-projection of dsLBs (magenta) and anchor 15bp and 25bp ssDNA (cyan). Scale bar is 50 µm. **C)** Representative confocal microscopy z-projection auf dsLB (magenta) assembly into constructs by anchor 15bp and 25bp ssDNA strands + corresponding linker 1a/1b. Scale bar is 500 µm. **D)** Representative bright field image of a construct assembled with 5 mol% 20bp ssDNA in the parallel plate micro-compression setup and the corresponding schematic illustration. **E) – G)** Maximal compression force measurement of constructs assembled from ssDNA with E) 15bp F) 20bp and G) 25bp at different ssDNA concentrations of 3 mol%, 5 mol% and 10 mol% using parallel micro-compression. Results are shown as ± SD of n <= 6 constructs. p values were calculated using two-tailed t test, ns = not significant $p > 0.05$, $^{*}p < 0.05$.

Towards introducing biochemical functionality into the constructs, we next coupled T cell-stimulating IgG antibodies, specifically anti-CD3 and anti-CD28, to the dsLB membrane *via*

View Article Online
DOI: 10.1039/D6SM00119J

lipids with maleimide headgroups **(Figure 3 A).** These immune-functionalized constructs are further referred to as synthetic tissues. Confocal microscopy imaging of an AlexaFluor488-conjugated IgG confirmed successful functionalization of the synthetic cell surface and no competitive binding of ssDNA and antibodies **(Figure 3 B)**. The functionalization of dsLB membranes with ssDNA enabled the formation of complex architectures based on the innate high specificity of DNA hybridization, allowing highly directed integration of multiple dsLB systems (plain, immune-stimulating, etc.), regardless of membrane components, into a single multi-zone synthetic tissue (**Figure 3 C**). Again, confocal microscopy imaging confirmed the formation of synthetic tissues with multiple zones of different constructs visualized by the ssDNA combination of anchor 20bp + linker 1b+1a-Cy3 (yellow) or linker 2b+2a-Cy5 (cyan) (**Figure 3 D**). Of note, we observed preserved structural integrity of constructs over a period of 2 weeks at 4 °C (**Figure S 2 A**). This approach leverages the high specificity of DNA hybridization and programmable ssDNA design to enable the construction of multicomponent, hierarchical constructs. These mimic the morphology and microanatomy of real tissues and comprise multiple distinct zones (**Figure 3 E**).

View Article Online
DOI: 10.1039/D6SM00119J

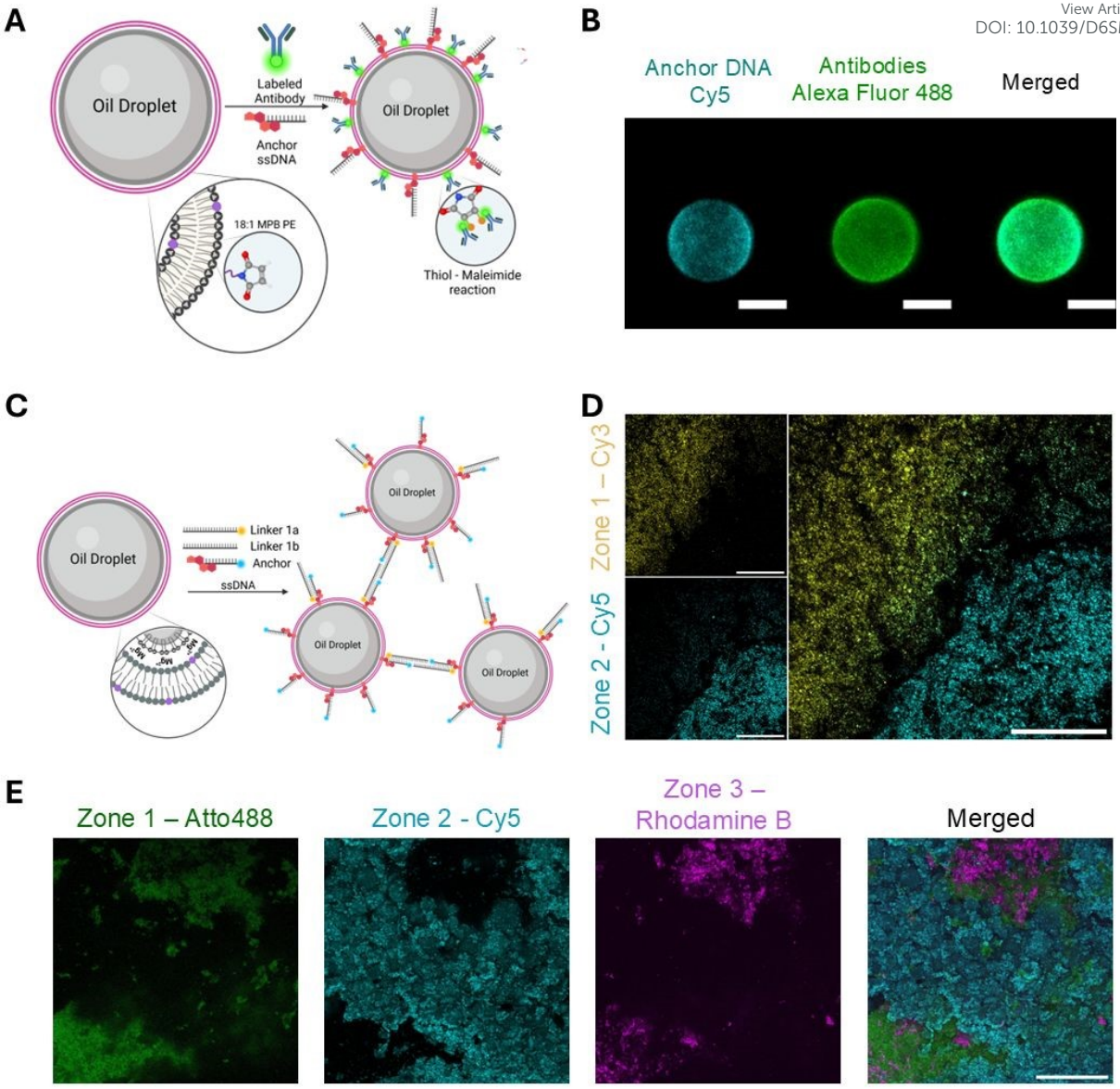

Figure 3: Zone formation for constructs and immune-functionalized synthetic tissues A) Schematic illustration of biochemical dsLB functionalization with antibodies *via* Thiol-Maleimide reactions. **B)** Representative confocal microscopy z-projection of anchor 20bp-Cy5 ssDNA strand (cyan) and Alexa Fluor 488 labelled antibodies (green). Scale bar is 5 µm. **C)** Schematic illustration of multi-zone construct formation using different linker ssDNA connections. **D)** Representative confocal microscopy z-projection of constructs formed and visualized by the ssDNA combination of anchor 20bp + linker 1b+1a-Cy3 (yellow) forming zone 1 or linker 2b+2a-Cy5 (cyan) forming zone 2. Scale bar is 250 µm. **E)** Representative confocal microscopy z-projection of multi-zone construct formation visualized by fluorophore-labelled lipids in the dsLB membrane: zone 1 – Atto 488 (dsLB membrane: green) formed with anchor 25bp + linker 1a/1b 25bp, zone 2 – Cy5 (dsLB membrane: cyan) formed with anchor 20bp + linker 1a/1b 20bp and zone 3 – Rhodamine B (dsLB membrane: magenta) formed with anchor 20bp + linker 2a/2b 20bp. Scale bar is 250 µm.

For high-throughput screenings or potential industrial applications, a more parallelized method for construct formation is required. To address this, we implemented a microwell plate formation approach. For this, each well of a 96-well plate served as a template for a “pancake” like construct covering the entire well (**Figure 4 A**). This strategy presents a more robust

View Article Online
DOI: 10.1039/D6SM00119J

method and allows to maximize contact formation between natural cells incubated within the synthetic tissue. Synthetic tissue formation and zone organization was confirmed for this setup by stereo- and confocal microscopy (**Figure 4 A, Figure 4 B**).

Next, we evaluated the applicability of DNA-based synthetic tissues as culturing system for living human immune cells from healthy donors. For this, we determined the DNA-based construct stability in cell culture medium. Confocal microscopy confirmed structural integrity of the constructs after 4 days in fully supplemented cell culture medium (**Figure S 2 B**). Furthermore, to verify the structural integrity of the constructs under cell culture conditions (i.e. cell culture medium enriched with DNase from serum components), we incubated constructs varying concentrations of DNase. We observed no construct disassembly at low (100 µg/mL) DNase concentrations after 4 days incubation at 37 °C in fully supplemented T cell medium. However, with higher (500 µg/mL) DNase concentrations the constructs disassembly. During construct disassembly, single dsLBs return to the dispersed state, thus increasing the apparent construct size and total dsLB covered area measured by microscopy. The total construct area doubled upon addition of 500 µg/mL DNase after 4 days of incubation which indicated decreased structural integrity. (**Figure S 2 C**). Additionally, immune-functionalized synthetic tissues remain structurally stable over 4 days of incubation in PBS at 4 °C or fully supplemented medium at 37 °C indicated by no changes in construct area (**Figure S 2 D**).

Finally, primary human $CD8^+$ T cells were seeded on the DNA-based immune-functionalized synthetic tissues and incubated for 4 days. The immune-functionalized synthetic tissues which host natural cells are also referred to as assembloids. Synthetic tissues with two distinct zones, one antibody-functionalized zone and one unfunctionalized scaffolding zone for structural support, were applied. The functionalized zones comprised 75% of the synthetic cell mix and the scaffolding zone 25%. For both zones, 5 mol% density of 20bp ssDNA on the synthetic cells was used. Staining for T cell nuclei after the incubation and inspection by confocal microscopy reveals clonal expansion clusters of T cell proliferated within the 3D assembloids after 4 days (**Figure 4 C**). Of note, our previous study revealed preferential co-localization of T cells in immune-functionalized zones [21]. Flow cytometry analysis of CD25 expression

View Article Online
DOI: 10.1039/D6SM00119J

confirmed the activation of T cells within the assembloids. The CD25 expression was benchmarked against the industry gold standard, Dynabeads. Both T cell activation approaches exhibited comparable activation rates of about 40% of the total T cell population. These results align with the T cell activation we observed in biotin-streptavidin lymphBUTs in our previous [8, 21], while T cells expanded in the assembloids also exhibited increased expression of the immunosuppressive receptor PD-1 (**Figure 4 D**).

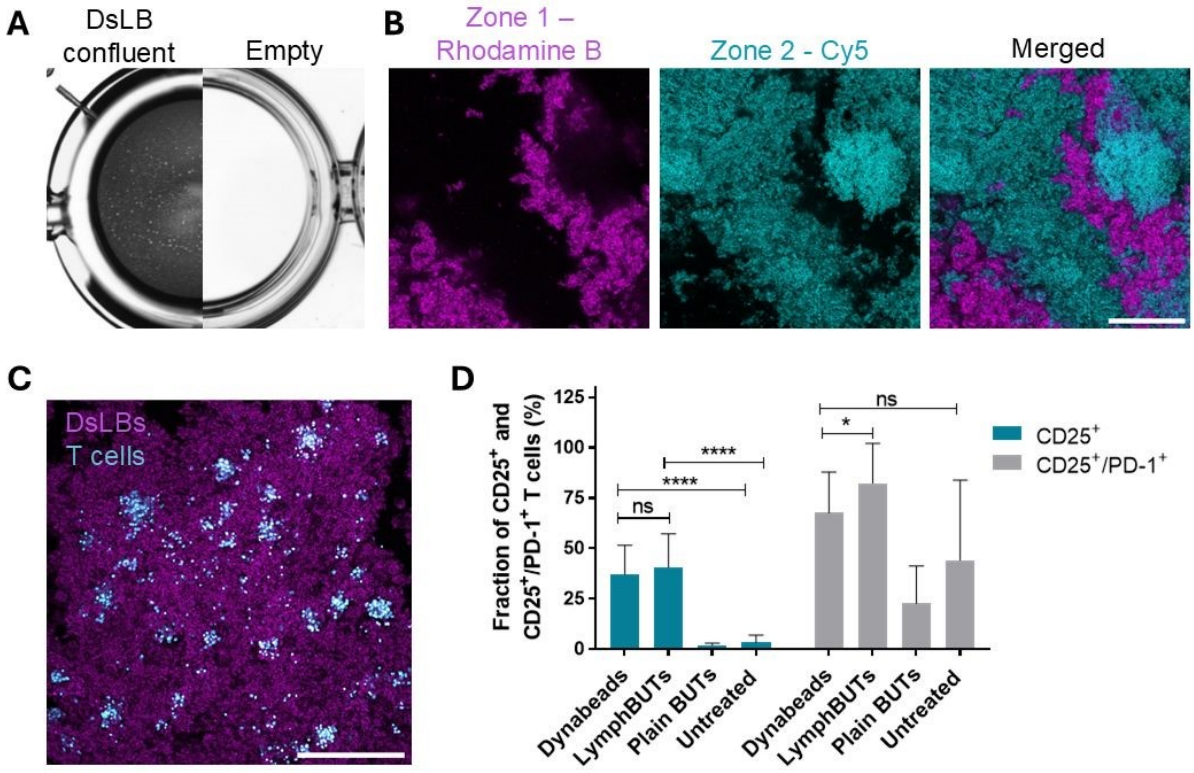

Figure 4: Synthetic tissue standardization and assembloid application A) Representative stereo microscope image of a dsLB confluent ("carpet" antibody functionalized constructs) and an empty 96 well. **B)** Representative confocal microscopy z-projection of multi-zone synthetic tissues visualized by fluorophore-labelled lipids in the dsLB membrane: zone 1 Rhodamine B (dsLB membrane: magenta) formed with anchor 20bp + linker 1a/1b and zone 2 Cy5 (dsLB membrane: cyan) formed with anchor 20bp + linker 2a/2b. Scale bar is 250 µm. **C)** Exemplary representative confocal microscopy z-projection of T cells (nuclei in cyan) infiltrated and formed clonal proliferation cluster within an assembloid formed with anchor 20bp + linker 1a/ab (dsLB membrane: magenta) after 4 days of co-cultivation. **D)** Quantification of the $CD25^+$ and $CD25^+/PD\text{-}1^+$ expressing T cell fraction expanded with Dynabeads or DNA-based assembloids measured by flow cytometry. Results are shown as mean ± SD of four donors in n > 2 technical replicates. p values were calculated using two-tailed t test. ns = not significant $p > 0.05$, $^{*}p < 0.05$, $^{****}p < 0.0001$.

View Article Online
DOI: 10.1039/D6SM00119J

Summary and discussion

In this study, we introduce a new approach for assembloid formation that enables controlled and reliable intercellular connections between individual synthetic cells. Inspired by approaches to engineer intercellular binding *via* ssDNA nanotechnology [33, 34], we designed multizonal synthetic tissues. Contrary to our previously established biotin-streptavidin approach, an almost covalent bond that is not programmable in structural self-assembly, partially complementary ssDNA enables the formation of multiple spatial zones in more defined and modular manner. Each zone can be equipped with a distinct protein or antibody portfolio precisely matching the biological requirements of the co-cultured natural cells, ultimately forming millimetre-sized synthetic tissues.

The use of ssDNA provides programmability beyond complementarity, enabling systematic control over strand length and surface density on the synthetic cells. This mirrors natural cell collectives, where cells dynamically regulate the expression level and type of adhesion molecules to control processes such as epithelial-mesenchymal transition [35]. Consistent with this concept, our results show that mechanical compressibility and therefore emergent mechanical construct properties, can be tuned through ssDNA surface density, in a minimalist manner. Additionally, we could characterize the relevance of DNA binding strength (i.e. linker length) and density, specifically for the 20bp linker length system with respect to lowest and highest ssDNA concentration of 2 and 20 mol%. Constructs formed with 2 mol% ssDNA tend to be mechanically more fragile, which was indicated by the lower indentation force needed to compress 10% of the total construct height. In contrast, we did not observe decreased structural stability of constructs formed with 20 mol% ssDNA while at the same time having low stiffness. We hypothesize that this either originates form incomplete incorporation of ssDNA in the dsLB membrane or steric hinderance by too many ssDNA strand in the inter-dsLB space. Additionally, DNA strand-displacement could be employed to restructure assembloids *in situ* and releasing the hosted natural cells without subjecting them to excessive mechanical stress.

View Article Online
DOI: 10.1039/D6SM00119J

Moreover, using ssDNA facilitates construct assembly under cell culture conditions, such as standard cell culture medium supplemented with serum, which commonly contains free biotin and therefore interferes with the biotin-streptavidin linkage. Also, the structural integrity of constructs and synthetic tissues in fully supplemented medium remains over the total incubation time of 4 days. By further implementing a 96-well plate compatible formation and culture format, we developed a faster, more standardized, and scalable platform capable of hosting cells within a 3D environment.

The hybridization and stability of ssDNA is primarily influenced by two major factors, cation concentration and the presence of digestive nuclease present in fetal bovine serum (FBS), thus making cell culture medium a harsh environment for DNA and especially ssDNA nanotechnology. Previous studies have shown that reducing FBS concentrations to 1% and increasing Mg^{2+} levels can prolong DNA stability [36]. Additionally, encapsulating DNA nanostructures within lipid bilayers has been reported to protect against nuclease-mediated digestion [37]. However, we observed stable ssDNA interactions, indicated by preserved synthetic tissue and zone integrity, for several days in fully supplemented cell culture medium and even for weeks under long term storing conditions (PBS, 4 °C). We hypothesize that the unexpectedly high stability originates from a synergistic combination of 1) enhanced stability by the lipid bilayer integration 2) respectively short ssDNA length, 3) locally enhanced Mg^{2+} concentration within the dsLB membrane, and 4) close proximity between the dsLBs membranes creating a DNase excluded zone.

We demonstrated biological applicability of these new 3D culture environments by using them to activate and expand primary human $CD8^+$ T cells. Their biological performance was benchmarked against commercially available activation beads (Dynabeads) as they are the established standard in both clinical and academic applications due to their strong and rapid activation and broad commercial availability. Thus, we successfully applied a self-assembling synthetic tissue which microanatomic organization is directed by partially complementary ssDNA hybridization. Particularly, the parallelized well plate formation approach, in which the single synthetic cells can function as “synthetic cell ink”, emphasizes the substantial potential

View Article Online
DOI: 10.1039/D6SM00119J

for future industrial and academic applications, including high-throughput drug or toxicity screenings. By tuning the biological functionality of individual synesthetic cells, synthetic tissues can function as custom-tailored 3D cell culture environments, not just for immune cells such as natural killer cells, neutrophils or lymphocytes but also for fibroblasts or stem cells.

Since construct formation *via* ssDNA hybridization enables the formation of assembloids in a well-defined and controlled manner, this approach builds a foundation for introducing synthetic cell morphogen gradients within a 3D environment [38]. To achieve this and to mimic structural and functional heterogeneity of biological organoids, additional synthetic cell types such as DNA-conjugated GUVs or coacervates can be incorporated, each leveraging their individual advantages to form emergent multicellular systems.

Experimental section

View Article Online
DOI: 10.1039/D6SM00119J

DsLB production

DsLBs were produced using the established and reported protocols [8, 21]. Briefly, 100 mg of PDMS (Sylgard 184, Dow Corning USA) were pre-emulsified in 900 µL of PBS (adjusted to pH 7 with HCl) and 4 mM of sodium dodecyl sulfate (SDS, Sigma–Aldrich, Germany). The oil in water pre-emulsion was further emulsified in a sonification bath for 2 min. By adding 22 mM of $MgCl_2$ (Sigma–Aldrich, Germany) a cationic layer was formed around the oil droplets which binds anionic small unilamellar vesicles (SUVs) of which 100 µL (6 mM) were added, mixed and incubated for 2 min protected from light. Excess SUVs were removed by three washing steps repeating centrifugation at 10000 xg for 30 sec, discharging of the supernatant and resuspension in PBS adjusted to pH 7.

The SUVs were produced using extrusion as described previously [8]. They consist of 20 mol% EggPG, 5 mol% 18:1 MPB PE (maleimide), 1 mol% LissRhodamine B-PE, Atto488-PE or 18:0 Cy5 PE and EggPC acting as a filling lipid (all Avanti Polar Lipids, USA).

DsLB immune functionalization

A maleimide functionalized lipid (Avanti Polar Lipids, USA) was integrated with 5 mol% in the SUVs and furthermore in the dsLB membrane enable the attachment of antibodies and proteins *via* thiol connections. To define the total accessible amount of maleimide in the dsLB membrane, a SUV 1:1 dilution series ranging from 60 µM to 0.47 µM was prepared in a 96-well plate and used for calibration. The dsLB suspension was diluted 1:10 with PBS into the well plate [8, 21].

The dsLB fluorescent intensity was measured with a TECAN Spark plate reader (Tecan Group, Switzerland) controlled by TECAN SparkControl software with in-built gain optimization. The

View Article Online
DOI: 10.1039/D6SM00119J

excitation/emission settings were adjusted to Rhodamine B (537/582 nm), Atto488-PE (495/545 nm) or CY5-PE (630/675 nm) labelled dsLBs [21].

Based on the total lipid membrane concentration and therefore accessible maleimide headgroups, the immune-stimulating antibodies against human CD3 (UCHT1, Invitrogen) and CD28 (CD28.2, Invitrogen) at a ratio (maleimide/antibody) of 0.5 high (~1020 molecules/μm^2) and a 1:3 ratio between αCD3/αCD28 were attached to the dsLB membrane. In order to remove sodium azide which, impacts the pH and therefore the efficiency of the thiol – maleimide reaction, the antibodies were washed using the MircoSpin™ G-25 Columns (Cytiva, US) according to manufacturer instructions. The washing leads to a reduction of antibody concentration of 9% (+/-1%) which was considered for all calculations. The dsLBs were incubated with the antibodies in PBS adjusted to pH 7 at RT for 1 h resuspending every 15 min. To get rid of un-bound antibodies the immune- dsLB were centrifuged at 10,000 xg for 30 sec and resuspended in PBS. The dsLB´s membrane concentration was adjusted to 150 – 300 µM with the help of the total lipid concentration measured using the plate reader [8, 21].

DsLB ssDNA functionalization and construct formation

By integrating single stranded DNA (ssDNA) *via* cholesterol residues into the antibody-functionalized dsLB membrane and subsequent addition of partly complementary linker DNA, single dsLBs can be connected into constructs in a very controlled manner. Following ssDNA strands, inspired by [39], were used driving the construct formation and are accordingly named in the main text.

Table 1: SsDNA sequences (5´ → 3´) with the corresponding name all purchased from Biomers GmbH, Germany

Name	Sequence 5' → 3'
Linker 1a 11bp	5'/TTCTTGTGAACACCTAGCTCTTTCACTATCTG/3'
Linker 1b 11bp	5'/TTCTTGTGAACCAGATAGTGAAAGAGCTAGGA/3'

View Article Online
DOI: 10.1039/D6SM00119J

Linker 1a 13bp mm	5'/CTTACTTGTGAACACCTAGCTCTTTCACTATCTG/3'
Linker 1b 13bp mm	5'/CTTACTTGTGAACCAGATAGTGAAAGAGCTAGGA/3'
Anchor 15bp-Cy5	Cy5/5'/GTTCACAAGAAAGCGTTTT/3'/Chol
Anchor 15bp	5'/GTTCACAAGAAAGCGTTTT/3'/Chol
Linker 1a 15bp	5'/CGCTTTCTTGTGAACACTCTTTCACTATCT/3'
Linker 1b 15bp	5'/CGCTTTCTTGTGAACAGATAGTGAAAGAGA/3'
Anchor 20bp	5'/GTTCACAAGAAAGCGGAAGCTTTT/3'/Chol
Anchor 20bp-Cy5	Cy5/5'/GTTCACAAGAAAGCGGAAGCTTTT/3'/Chol
Linker 1a 20bp-Cy3	Cy3/5'/GCTTCCGCTTTCTTGTGAACACCTAGCTCTTTCACTATCTG/3'
Linker1a 20bp	5'/GCTTCCGCTTTCTTGTGAACACCTAGCTCTTTCACTATCTG/3'
Linker 1b 20bp	5'/GCTTCCGCTTTCTTGTGAACCAGATAGTGAAAGAGCTAGGA/3'
Linker 2a 20bp-Cy5	Cy5/5'/GCTTCCGCTTTCTTGTGAACACTGATCTAATGGTGCACGTT/3'
Linker 2a 20bp	5'/GCTTCCGCTTTCTTGTGAACACTGATCTAATGGTGCACGTT/3'
Linker 2b 20bp	5'/GCTTCCGCTTTCTTGTGAACAACGTGCACCATTAGATCAGA/3'
Anchor 25bp-Cy5	Cy5/5'/GTTCACAGATGAAGAAAGCGGAAGCTTTT/3'/Chol
Anchor 25bp	5'/GTTCACAGATGAAGAAAGCGGAAGCTTTT/3'/Chol
Linker 1a 25bp	5'/GCTTCCGCTTTCTTCATCTGTGAACACCTAGCTCTTACGCATCACTATCTG/3'
Linker 1b 25bp	5'/GCTTCCGCTTTCTTCATCTGTGAACCAGATAGTGATGCGTAAGAGCTAGGA/3'
Dis strand	5'/AAAGCTTCCGCTTTCTTGTGAAC/3'

Single stranded DNA (ssDNA) was functionalized with cholesterol in order to integrate the anchor ssDNA into the dsLB membrane *via* self-assembly in concentrations ranging from 2 – 20 mol% based on the total lipid membrane concentration determined as previously described. To achieve lymphBUT formation, the highly concentrated dsLBs (150 – 300 µM) were incubated with the anchor ssDNA as well as ssDNA linker a and ssDNA linker b using a ratio equimolar ratio of 1:1:1 for 1 h at RT within a 0.5 mL microtube. The total reaction volume was kept between 20 – 50 µL. During the incubation period the microtube was placed upside down to prevent dsLB loss due to sticking to the tube walls, facilitating construct formation at the

View Article Online
DOI: 10.1039/D6SM00119J

PBS/air interface. To produce consistently sized constructs 40 µL of a 150 µM dsLBs solution was constant over the experiments. The total lipid concentration was determined as previously described. The formed constructs were gently flushed with 200 µL of PBS or cell culture medium and allowed to rest for another 1 h at RT.

Multi-zone construct formation

Multi-zone constructs were assembled through a sequential process in which multiple dsLB or construct subunits were connected to yield a single, continuous, functional construct. Each subunit can be formed form differently functionalized dsLBs carrying immune-stimulating antibodies or different membrane fluorophores, as well as labelled ssDNA strands and ssDNA strands length of 15bp, 20bp or 25bp. Assembly was performed in either PBS adjusted to pH 7 or in cell culture medium, as specified below.

Microtube formation method: For the multi-zone construct formation subunits were either formed with (activating zone) or without (scaffolding zone) immune-stimulating antibodies in separate 0.5 mL Eppendorf tubes. Briefly, we applied a sequential addition approach where partially adding linker a and linker b to dsLBs already leads to the formation of sub-zonal constructs. After combining those sub-zonal constructs the rest of the linker a and b is added to reach the aimed ratio of anchor: linker a and linker b. This formation happens in four steps and results in rounded sphere-like geometries.

Step 1: The dsLB membrane was functionalized with anchor ssDNA (5 mol% of the total lipid membrane) and anchor ssDNA was partially saturated (50%) with linker a and b ssDNA. This mixture was incubated for 30 min in a total reaction volume of 20 -50 µL.

Step 2: Subsequently, the formed constructs were flushed with either 200 µL of sterile PBS or cell culture medium and incubated at RT for 1h.

Step 3: The activating and the scaffolding subunits were combined in one 0.5 mL Eppendorf tube and excess PBS or cell culture medium was removed to obtain a final volume of ~50 µL.

View Article Online
DOI: 10.1039/D6SM00119J

To initiate the inter-subunit connection, the second 50% of linker a and b of ssDNA was added to achieve a 1:1:1 ratio of anchor:linker a:linker b.

Step 4: The Eppendorf tube was incubated upside down, protected from light, for 1 h at RT. The resulting multi-zone constructs were subsequently washed by flushing with 200 µL of PBS or cell culture medium and stored at 4 °C until further use.

Well plate formation method: For the combination of multiple dsLB subtypes into a multi-zone dsLB agglomerate a flat-bottom 96-well plate served as a physical template that promoted planar pancake-like construct formation. Immuno-functionalized dsLBs (75% of the synthetic tissue) and plain dsLBs (25% of the synthetic tissue) were mixed with anchor and both linker ssDNA in individual microtubes before being transferred dropwise into the 96 well. Each drop later presents a zone. The ssDNA concentration for cell culture experiments was always 5 mol% and a ssDNA length of 20bp. The dsLBs mixtures formed into synthetic tissues after 1 h incubation at RT protected from light. The synthetic tissues can then be stored at 4 °C until further use.

Laser scanning confocal microscopy imaging of constructs

The fluorescently labelled dsLB membrane and labelled ssDNA as well as dsLB agglomerate referred to as constructs or assembloids were visualized using the confocal laser scanning microscope LSM 880 (Carl Zeiss AB) equipped with a 10x objective (EC "Plan-Neofluar" 10x/0.30 M27, Carl Zeiss AG, Germany) and 63x immersion oil objective (Plan-Apochromat 63x/1.4 oil DIC M27, Carl Zeiss AG, Germany) with the 405, 488 and 633 laser lines. The primary human $CD8^+$ T cells were fixed with 2% PFA for 30 min and the T cell nucleus was stained with Hoechst 33342 trihydrochloride (Thermo Fisher, Germany). For this the fixed T cells were incubated with 1µM Hoechst 33342 for 30 min and washed by replacing half of the volume three times. The images were analysed with the ImageJ software (NIH, USA) by snaps or z-projection of stacks and background subtraction [8, 21].

View Article Online
DOI: 10.1039/D6SM00119J

Construct disassembly using ssDNA higher affinity displacement strands

Constructs were assembled following previously described protocols using anchor 20bp and linker 11bp or 13bp mm ssDNA strands. To perform strand displacement the environmental ionic strength from PBS or cell culture medium needs to be reduced. For this the constructs were washed by two times sequential exchange of PBS/medium by ddH_2O and subsequently incubated for 30 min at RT. For construct disassembly, a higher affinity ssDNA strand complementary to the anchor strand (disassembly strand, “Dis strand”) was added in 200% of the anchor. The samples were monitored over 45 min at 37 °C in a 1 min interval *via* confocal laser scanning microscope LSM 880 (Carl Zeiss AB).

Mechanical construct properties

Micro-compression was used to evaluate the mechanical properties of lymphBUT formed with different ssDNA concentrations (2 mol%, 3 mol%, 5 mol%, 10 mol% and 20 mol%) as well as different ssDNA length (15bp, 20bp, 25bp). For this, the constructs were transferred onto a testing anvil within a CellScale fluid bath filled with 45 mL. The cantilever was assembly manually by glueing a 1x1 mm square stainless-steel platen to a tungsten microbeam with a diameter of 0.0762 mm and a modulus of 411000 MPa which was mounted into the Microindenter G2 CellScale (CellScale biomaterials testing, Canada). The constructs were compressed with a compression magnitude of 10% of the total construct height measuring the indentation force. The z-compression was controlled in a ramp setting with a loading duration of 30 sec, a holding duration of 5 sec and a recovery duration of 30 sec. Real time imaging was performed with a USB digital camera with a zoom lens and XYZ automated stage tracked at a frequency of 5 Hz [21].

T cell isolation and cultivation

View Article Online
DOI: 10.1039/D6SM00119J

Functional assays were performed with primary human CD8⁺ T cells. The T cells were isolated from leukapheresis reduction system chambers from healthy voluntary blood donors using negative isolation. The isolation was performed with commercial selection kits (RosetteSep Human CD8⁺ T cell Enrichment Cocktail, STEMCELL technologies, Germany) following the manufacturers instruction. The blood was provided by the Institute for Clinical Hemostaseology and Transfusion Medicine, Saarland University Medical Center provided the blood according to the ethics agreement number 34/23 (Ethikkommission Ärztekammer des Saarlandes). The isolated CD8⁺ T cells were stored in RPMI 1640 w/ L-Glutamine (VWR, Germany) medium supplemented with 40% fetal bovine serum (Gibco, Germany), 1% penicillin/streptomycin (Gibco, Germany), 1% non-essential amino acids (Biowest) and 50 mM HEPES (Sigma–Aldrich, Germany) and additional 10% dimethyl sulfoxide (DMSO) (Sigma Aldrich, Germany) and stored at -80 °C until further use [8, 21].

The primary human CD8⁺ were thawed and cultivated overnight in RPMI 1640 w/L-Glutamine (VWR, Germany) medium supplemented with 10% fetal bovine serum (Gibco, Germany), 1% penicillin/streptomycin (Gibco, Germany), 1% non-essential amino acids (Biowest, France) and 50 mM HEPES (Sigma–Aldrich, Germany) with 100 U mL^{-1} of the growth factor Interleukin 2 (IL-2) in T 25 cell culture flasks at 37 C and 5% CO_2 [8, 21].

T cell *ex vivo* activation and expansion within synthetic tissues

100,000 – 120,000 isolated CD8⁺ T cells were added to the synthetic tissues produced according to the well plate formation method and filled with fully supplemented medium to a total volume of 200 µL and a total IL-2 concentration of 100 U mL^{-1}. The cells were then co-cultivated at 37 °C and 5% CO_2 for 4 days with the synthetic tissues. The wells at the outer border were filled with PBS in order to avoid evaporation and therefore biased results. Dynabeads human T-Activator CD3/CD28 beads (Gibco, Germany) used according to manufacturer suggestions served as controls [21].

View Article Online
DOI: 10.1039/D6SM00119J

CD8⁺ T cell activation studies using Flow Cytometry

To further study primary human CD8⁺ T cell activation and immunosuppression signal the assembloids were resuspended in order to separate dsLBs and T cells and centrifuged at 300 xg for 5 min. The supernatant was disposed and the cells were resuspended in PBS + 1% Albumin fraction V (BSA) (Sigma–Aldrich, Germany) containing staining antibodies (1:400) against the surface marker CD25 (BC96, BioLegend, UK) and PD-1 (NAT105, BioLegend, UK) conjugated to Alexa Fluor 488 or Alexa Fluor 647. The cells were stained with the antibodies for 1 h at RT protected from light. Subsequently the cells were washed once with PBS, resuspended in PBS containing 2% PFA (Sigma–Aldrich, Germany) and incubated for 30 min at RT protected from light followed by washing step with PBS. After disposing the remaining PFA the cells were resuspended in PBS containing 1 nM Hoechst 33342 trihydrochloride (Thermo Fisher, Germany) for staining the T cell nucleus for 30 min protected from light. Finally, the cells were washed once more and resuspended in PBS + 1 BSA and resuspended in a final volume of 200 µL PBS + 1% BSA and stored at 4 °C until further flow cytometer measurements. For the quantification of the surface marker the Attune NxT Flow Cytometer and with the Attune™ Software (Thermo Fisher, Germany) and equipped with 405, 488, 561 and 637 nm laser lines were used. For the analysis a minimum of 10,000 events were considered and analysed with the FlowJo V.10 software (FlowJo LLC, USA) [8, 21].

Shelf-life stability of multi-zone constructs

Multi-zone construct formation is based on surface interactions induced by complementary ssDNA between the activating and scaffolding zones. The time dependent structural and mechanical stability of multi-zone constructs was evaluated by confocal microscopy. For this, constructs made from two zones visualized with either Cy5 or Cy3 labelled linker ssDNA were formed as previously described and transferred to a 48-well suspension plate with 200 µL of PBS. The constructs were evaluated according to their mechanical stability and zone integrity over 2 weeks (n=2).

View Article Online
DOI: 10.1039/D6SM00119J

Metabolic degradation resistance of ssDNA constructs and synthetic tissues in cell culture medium

SsDNA used for construct formation could potentially be targeted for degradation by e.g. nucleases in the cell culture medium, thus leading to structural disassembly of the constructs and synthetic tissues. To evaluate this, constructs and synthetic tissues were formed in Eppendorf tubes with 5 mol% and 20bp ssDNA, transferred to 48-well plates and stored in fully supplemented RPMI 1640 medium over 4 days at 37 °C or in PBS at 4 °C. Structural stability was analysed *via* confocal microscopy for 4 days ever 24 h (n=4) and the LEICA DFC450 stereo microscope (Leica Microsystems, Germany) and a 2x (PLANAPO 2.0x/39, Leica Microsystems, Germany) or a 5x objective (PLANAPO 5.0x/0.5, Leica Microsystems, Germany). Stereo microscopic images were analysed as mentioned below.

Furthermore, constructs produced with the well-plate strategy and incubated in fully supplemented RPMI 1640 medium with additional 100 µg/mL and 500 µg/mL DNase I (Roche Diagnostics GmbH, Germany) at 37 °C for 1h and 96 h. The constructs structural integrity was evaluated by the total construct area imaged with a LEICA DFC450 stereo microscope (Leica Microsystems, Germany) and a 2x (PLANAPO 2.0x/39, Leica Microsystems, Germany) or a 5x objective (PLANAPO 5.0x/0.5, Leica Microsystems, Germany). The images were analysed with the ImageJ software (NIH, USA) by global-threshold segmentation and automated particle detection. Low structural integrity was identified by increasing total construct area.

Data processing and statistical analysis

Graphs were plotted with GraphPad Prism 7 as mean +/- SD of technical and biological replicates. Statistical analyses were performed with the in-build GraphPad Prism 7 software function. The applied statistical analysis was noted for the individual figures in the figure legends. Schematic illustrations were created with BioRender.com [8, 21].

View Article Online
DOI: 10.1039/D6SM00119J

Acknowledgements

The authors thank the INM Fluorescence Microscopy Core Facility and Cao Nguyen Duong (Leibniz Institute for New Materials) for the confocal microscope use. We also thank Kathleen Seelert (CIPMM) for her help with blood and T cell handling and collection. The authors acknowledge funding from the Pharmazeutische Forschungsallianz Saarland, the Daimler and Benz Foundation (32-12/22), the Joachim Herz Foundation (Add-on Fellowship and Innovate! Akademie) and German Science Foundation (Emmy Noether Program, project number 525255627 and 545610076).

Competing interests

The authors declare no competing interests.

Authors contributions

A.B. performed and designed experiments, analysed the data, supervised experimental implementation and wrote the manuscript. E.A.L.L. performed experiments and analysed data. G.M.H. performed experiments and analysed data. K.J. designed the ssDNA and helped in protocol development. O.S. designed the study, supervised the experimental implementation and wrote the manuscript.

View Article Online
DOI: 10.1039/D6SM00119J

References

[1] H. Bayley, I. Cazimoglu, C.E.G. Hoskin, Synthetic tissues, Emerg Top Life Sci 3(5) (2019) 615-622.
[2] A.J. Lin, A.Z. Sihorwala, B. Belardi, Engineering Tissue-Scale Properties with Synthetic Cells: Forging One from Many, ACS Synth Biol 12(7) (2023) 1889-1907.
[3] J.E. Hernandez Bucher, O. Staufer, L. Ostertag, U. Mersdorf, I. Platzman, J.P. Spatz, Bottom-up assembly of target-specific cytotoxic synthetic cells, Biomaterials 285 (2022) 121522.
[4] O. Staufer, S. Antona, D. Zhang, J. Csatari, M. Schroter, J.W. Janiesch, S. Fabritz, I. Berger, I. Platzman, J.P. Spatz, Microfluidic production and characterization of biofunctionalized giant unilamellar vesicles for targeted intracellular cargo delivery, Biomaterials 264 (2021) 120203.
[5] J.H. Park, A. Galanti, I. Ayling, S. Rochat, M.S. Workentin, P. Gobbo, Colloidosomes as a Protocell Model: Engineering Life-Like Behaviour through Organic Chemistry, European Journal of Organic Chemistry 2022(43) (2022).
[6] Z. Lin, T. Beneyton, J.C. Baret, N. Martin, Coacervate Droplets for Synthetic Cells, Small Methods 7(12) (2023) e2300496.
[7] M. Valentini, S. Di Stefano, J. Boekhoven, Coacervate-Droplet Cased Synthetic Cells Regulated By Activated Carboxylic Acids (ACAs), ChemSystemsChem 7(3) (2024).
[8] A. Burgstaller, N. Piernitzki, N. Kuchler, M. Koch, T. Kister, H. Eichler, T. Kraus, E.C. Schwarz, M.L. Dustin, F. Lautenschlager, O. Staufer, Soft Synthetic Cells with Mobile Membrane Ligands for Ex Vivo Expansion of Therapy-Relevant T Cell Phenotypes, Small (2024) e2401844.
[9] N. Piernitzki, N. Gao, G. Gasparoni, L.M. Krauss, J. Schulze-Hentrich, M. Dustin, B. Schrul, B. Gyorffy, S. Mann, O. Staufer, Self-assembly of hybrid 3D cultures by integrating living and synthetic cells, Nat Commun 16(1) (2025) 11073.
[10] N. Yandrapalli, Bottom-up development of lipid-based synthetic cells for practical applications, Trends Biotechnol 43(9) (2025) 2150-2169.
[11] A.J. Engler, S. Sen, H.L. Sweeney, D.E. Discher, Matrix elasticity directs stem cell lineage specification, Cell 126(4) (2006) 677-89.
[12] O.W. Petersen, Interaction with basement membrane serves to rapidly distinguish growth and differentiation pattern of normal and malignant human brestepithelial cells, Cell Biology Vol. 89, pp. 9064-9068 (1993).
[13] G.P. Raeber, M.P. Lutolf, J.A. Hubbell, Mechanisms of 3-D migration and matrix remodeling of fibroblasts within artificial ECMs, Acta Biomater 3(5) (2007) 615-29.
[14] H. Tanaka, C.L. Murphy, C. Murphy, M. Kimura, S. Kawai, J.M. Polak, Chondrogenic differentiation of murine embryonic stem cells: effects of culture conditions and dexamethasone, J Cell Biochem 93(3) (2004) 454-62.
[15] S.P. Pasca, P. Arlotta, H.S. Bateup, J.G. Camp, S. Cappello, F.H. Gage, J.A. Knoblich, A.R. Kriegstein, M.A. Lancaster, G.L. Ming, G. Novarino, H. Okano, M. Parmar, I.H. Park, O. Reiner, H. Song, L. Studer, J. Takahashi, S. Temple, G. Testa, B. Treutlein, F.M. Vaccarino, P. Vanderhaeghen, T. Young-Pearse, A framework for neural organoids, assembloids and transplantation studies, Nature 639(8054) (2025) 315-320.
[16] A. Burgstaller, S. Madureira, O. Staufer, Synthetic cells in tissue engineering, Curr Opin Biotechnol 92 (2025) 103252.
[17] V.S. LeBleu, Structure and Function of Basement Membranes, Experimental Biology and Medicine 232(9) (2007) 1121 - 1129.
[18] A. Passaniti, H.K. Kleinman, G.R. Martin, Matrigel: history/background, uses, and future applications, J Cell Commun Signal 16(4) (2022) 621-626.
[19] C.S. Hughes, L.M. Postovit, G.A. Lajoie, Matrigel: a complex protein mixture required for optimal growth of cell culture, Proteomics 10(9) (2010) 1886-90.
[20] E.A. Aisenbrey, W.L. Murphy, Synthetic alternatives to Matrigel, Nat Rev Mater 5(7) (2020) 539-551.
[21] A. Burgstaller, T. Nink, N. Walter, E.A.L. Lopez, H.F. Chang, O. Staufer, Synthetic Cell-Based Tissues for Bottom-Up Assembly of Artificial Lymphatic Organs, Adv Healthc Mater (2025) e03498.

[22] P. Yang, G. Boer, F. Snow, A. Williamson, S. Cheeseman, R.M. Samarasinghe, A. Rifai, A. Privam, R. Elnathan, R. Guijt, A. Quigley, R. Kaspa, D.R. Nisbet, R.J. Williams, Test and tune: evaluating, adjusting and optimising the stiffness of hydrogels to influence cell fate, Chemical Engineering Journal 505 (2025).
[23] R. Bhatta, J. Han, Y. Liu, Y. Bo, H. Wang, T cell-responsive macroporous hydrogels for in situ T cell expansion and enhanced antitumor efficacy, Biomaterials 293 (2023) 121972.
[24] H. Cao, L. Duan, Y. Zhang, J. Cao, K. Zhang, Current hydrogel advances in physicochemical and biological response-driven biomedical application diversity, Signal Transduct Target Ther 6(1) (2021) 426.
[25] S.B. Anderson, C.C. Lin, D.V. Kuntzler, K.S. Anseth, The performance of human mesenchymal stem cells encapsulated in cell-degradable polymer-peptide hydrogels, Biomaterials 32(14) (2011) 3564-74.
[26] O. Chaudhuri, L. Gu, D. Klumpers, M. Darnell, S.A. Bencherif, J.C. Weaver, N. Huebsch, H.P. Lee, E. Lippens, G.N. Duda, D.J. Mooney, Hydrogels with tunable stress relaxation regulate stem cell fate and activity, Nat Mater 15(3) (2016) 326-34.
[27] A. Alcinesio, I. Cazimoglu, G.R. Kimmerly, V. Restrepo Schild, R. Krishna Kumar, H. Bayley, Modular Synthetic Tissues from 3D-Printed Building Blocks, Advanced Functional Materials 32(7) (2021).
[28] G. Villar, A.D. Graham, H. Bayley, A tissue-like printed material, Science 340(6128) (2013) 48-52.
[29] X. Huang, M. Skowicki, I.A. Dinu, C.A. Schoenenberger, C.G. Palivan, Stimuli-Responsive Prototissues via DNA-Mediated Self-Assembly of Polymer Giant Unilamellar Vesicles, Advanced Functional Materials 34(48) (2024).
[30] R. Luo, K. Göpfrich, I. Platzman, J.P. Spatz, DNA-Based Assembly of Multi-Compartment Polymersome Networks, Advanced Functional Materials 30(46) (2020).
[31] L. M, R. S, Cyanine dyes in biophysical research: the photophysics of polymethine fluorescent dyes in biomolecular environments, Quarterly Reviews of Biophysics 44(1) (2011) 123-151.
[32] N. Kretschy, M. Sack, M.M. Somoza, Sequence-Dependent Fluorescence of Cy3- and Cy5-Labeled Double-Stranded DNA, Bioconjug Chem 27(3) (2016) 840-8.
[33] Y. Sun, L. Xu, Y. Qian, X. Xiong, L. Li, Spatially Defined DNA Origami Cell Engagers for T and Natural Killer Cell-Mediated Immune Modulation, ACS Nano 20(13) (2026) 10320-10330.
[34] S. Ganguly, S. Roy, A.P. Goodwin, J.N. Cha, Generation of 3D cellular spheroids using DNA modified cell receptors and programmable DNA interactions, Biomater Sci 9(23) (2021) 7911-7920.
[35] C.Y. Loh, J.Y. Chai, T.F. Tang, W.F. Wong, G. Sethi, M.K. Shanmugam, P.P. Chong, C.Y. Looi, The E-Cadherin and N-Cadherin Switch in Epithelial-to-Mesenchymal Transition: Signaling, Therapeutic Implications, and Challenges, Cells 8(10) (2019).
[36] J. Hahn, Addressing the Instability of DNA Nanostructures in Tissue Culture, ACS Nano Vol 8/Issue 9 (2014) 8765-8775.
[37] S.D. Perrault, Virus-inspired Membrane Encapsulation of DNA nanostructures to Achieve in vivo Stability, ACS Nano Vol8/Issue 5 (2014) 5132-5140.
[38] L. Tian, M. Li, A.J. Patil, B.W. Drinkwater, S. Mann, Artificial morphogen-mediated differentiation in synthetic protocells, Nat Commun 10(1) (2019) 3321.
[39] A. Schoenit, C. Lo Giudice, N. Hahnen, D. Ollech, K. Jahnke, K. Gopfrich, E.A. Cavalcanti-Adam, Tuning Epithelial Cell-Cell Adhesion and Collective Dynamics with Functional DNA-E-Cadherin Hybrid Linkers, Nano Lett 22(1) (2022) 302-310.

View Article Online
DOI: 10.1039/D6SM00119J

Data availability statement

All data underlaying this study is available in the figures or supplementary information. No specific analysis code or software has been developed for this study and no publicly available data has been used.